Tilted Fiber Bragg Grating Measurements During Laser Ablation of Hepatic Tissues: Quasi-Distributed Temperature Reconstruction and Cladding Mode Resonances Analysis

Sanzhar Korganbayev, *Member, IEEE*, Martina De Landro, *Member, IEEE*, Alexey Wolf, Daniele Tosi, and Paola Saccomandi, *Senior Member, IEEE*

***Abstract*—In this work, we investigate the application of tilted fiber Bragg grating (TFBG) sensors during *ex vivo* laser ablation of porcine hepatic tissues. Initially, TFBG's ability to measure the surrounding refractive index (RI) for different sucrose concentrations and the possibility to measure the RI of the targeted tissue during laser ablation (LA) is analyzed. After, the temperature sensing modality of TFBG is investigated in detail. We have implemented an algorithm for quasi-distributed spatial temperature profile reconstruction along TFBG. The algorithm models the TFBG core mode spectrum as a chain of Bragg gratings (each Bragg grating is modeled *via* coupled mode theory), where each grating is sensitive to local temperature changes. After, the Gaussian-shape temperature profile along the TFBG is reconstructed using the iterative optimization technique. Temperature measurements have been compared with highly-dense FBG array measurements and with conventional TFBG point temperature measurements based on the core mode tracking techniques (maximum tracking, X-dB Bandwidth, centroid methods). Overall, the proposed reconstruction algorithm is able to provide a quasi-distributed temperature profile along TFBG, which is not possible to obtain using conventional point temperature measurements based on the TFBG's core mode tracking. The resulted root-mean-square error in comparison to FBG array reference measurements is 7.8±1.7 °C. In general, the results show that the main reliable sensing modality of TFBG during LA is temperature monitoring, which can be significantly improved by the proposed algorithm.**

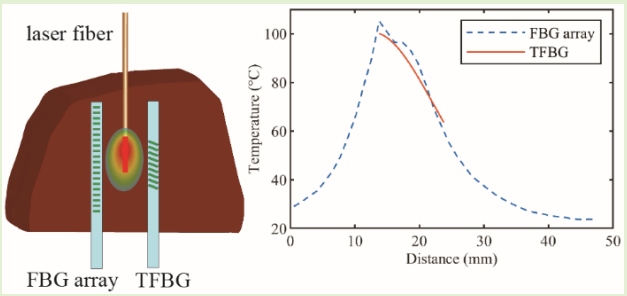

***Index Terms*—Laser ablation, optical fiber sensors, refractive index sensing, temperature monitoring, thermal treatment, tilted fiber Bragg grating.**

I. Introduction

HYPERTHMAL techniques can be considered as one of the main alternatives to traditional methods (surgical resection, chemotherapy, and radiation therapy) for cancer treatment [1], [2]. During such techniques, the tissue temperature increase is induced to destroy cancer cells, or sensitize tumors for radiotherapy and chemotherapy, or as complementary to cancer immune therapy [3]. Hyperthermia can be divided into several types according to the value of temperature elevation: fever-range (39.5 °C – 41.5 °C), traditional (41.5 °C – 54 °C), and ablation (more than 60 °C) [4]. Moreover, hyperthermia can be categorized according to the way of treatment (invasive or non-invasive), and by the source of energy: microwave [5], radiofrequency [6], high-intensity focused ultrasound [7], and laser ablation (LA), and others [8].

Among all invasive hyperthermal techniques, laser ablation possesses unique features such as immunity to electromagnetic interference and the ability to reach deep-lying organs. These advantages stem from the fact that the energy is guided by flexible optical fiber made of glass or polymer [9]. As a result, an effective treatment that is compatible with magnetic resonance and computed tomography guidance is possible. Different research works have been performed to validate the efficiency of LA treatment for thyroid [10], brain [11], pancreas [12], bones [13], and liver [14].

Manuscript received 10 June 2022; revised 5 July 2022; accepted 5 July 2022. Date of publication 13 July 2022; date of current version 15 August 2022. This work was supported in part by the European Research Council (ERC) under the European Union's Horizon 2020 Research and Innovation Program under Grant 759159 and in part by the Fondazione Cariplo under Grant 2017-2075. The work of Alexey Wolf was supported by the State Budget of the Russian Federation through the IA&E SB RAS Project under Grant 121030500067-5. The work of Daniele Tosi was supported by Nazarbayev University through SMARTER and EPICGuide under Grant 091019CRP2117 and Grant 240919FD3908. The associate editor coordinating the review of this article and approving it for publication was Prof. Carlos Marques. *(Corresponding authors: Sanzhar Korganbayev; Paola Saccomandi.)*

Please see the Acknowledgment section of this article for the author affiliations.

Digital Object Identifier 10.1109/JSEN.2022.3189153

Nevertheless, for the effective result of LA treatment without recurrences, irreversible damage to the whole cancer tissue has to be performed. Therefore, accurate monitoring of temperature and related tissue changes of the targeting tumor is of paramount importance [15]. In this regard, conventional invasive temperature monitoring methods, such as thermocouples [16], and thermistor probes [17], have two main limitations: the low spatial resolution and the metallic material of the devices. The low resolution of the sensors can not provide accurate temperature information due to high thermal gradients associated with LA, especially near the applicator [18]. The metallic material significantly absorbs the laser light, which leads to a change of heat distribution near the applicator and significant temperature overestimation (error can reach more than 20 °C) [9], [19].

Fiber optic sensing is one of the possible alternatives to conventional sensors for LA monitoring, due to their flexibility, sub-millimetric size, biocompatibility and immunity to electromagnetic interferences [18]. Moreover, fiber sensing is able to provide distributed (the whole fiber is a sensor) or quasi-distributed (fiber has several sensing points along its length) temperature measurements [20].

The most popular technique for distributed sensing during LA relies on Rayleigh scattering phenomena: temperature profile reconstruction is based on the analysis of spectral shift on each segment of the fiber between the measured and reference (no temperature change) states [21]. Rayleigh-based distributed sensing provides high sensing length, but its low spatial resolution, high interrogator cost, and low sampling rate limit its application for real-time monitoring during LA [20]–[22].

Quasi-distributed sensing is mainly based on fiber Bragg grating (FBG) temperature sensors. An FBG is a periodic modulation (with a specific grating period) of the refractive index along the fiber core. FBG acts as an optical narrowband notch filter: it transmits the whole input spectrum except the specific part of it. This portion is reflected from the FBG and centered at the Bragg wavelength [23]. Since the Bragg wavelength depends on temperature perturbations on the grating, monitoring of FBG peak can be used to measure temperature change at the grating [23].

Moreover, several FBGs with different grating periods can be inscribed along the fiber to obtain a spectrum with several different reflected Bragg wavelengths. The peak tracking of such spectra allows multi-point measurements (thus, the quasi-distributed sensing) along the chain of FBGs, called an FBG array.

The ability to provide multi-point measurements and immunity to electromagnetic interference pave the way for FBG sensing applications for laser hyperthermia [24]–[27]. Moreover, our group has recently demonstrated the efficacy of FBGs to regulate LA in real-time for maximum temperature control [28], zone control [29] during contactless LA, and temperature control during interstitial LA [30], [31] of *ex vivo* tissues.

A particular type of FBG is the tilted FBG (TFBG), in which the Bragg grating planes are tilted to the optical fiber axis. Due to the tilt of the grating and the related coupling between the core and cladding modes, TFBG is sensitive to fiber-related parameters (temperature, axial strain, pressure, bending, among others) and outside medium parameters, such as surrounding refractive index (RI) [32]–[35]. TFBGs have also been proposed for the simultaneous measurement of different quantities, benefiting from the difference in responses of cladding modes and core mode in the TFBG spectrum [36].

Recently, Alqarni *et al.* have used a TFBG structure to manufacture a self-monitored laser-irradiating device based on the application of TFBG with an absorptive coating as a miniature heat source with sensing capabilities [4]. In this case, the tilt angle of the grating leads to the light coupling to cladding modes and absorption of it by coating. Thus, this technique is not based on laser absorption by the tissue, but on heat transfer from the absorptive coating surface of TFBG. Temperature monitoring in [4] is based on conventional TFBG core mode tracking, in which TFBG acts as a sensing point and allows only a single-point measurement.

Considering the multi-sensing capabilities of the TFBG and its potential application in LA, it is useful to explore the possibility to use different TFBG sensing modalities for thermal treatment monitoring and improve TFBG temperature measurement capabilities.

In this regard, we investigate TFBG's ability to measure surrounding RI, which can be an important parameter to obtain information about the composition of tissues with which the TFBG sensor comes into contact. Indeed, the light propagation within tissue is sensitive to changes in medium microstructure, hence optical parameters could be used to directly quantify the tissue damage [37], [38]. It is known that the RI values of biological tissues are primarily mapped by their water content: the higher the content of water in the tissue, the closer its RI value to that of water (RI=1.33) and vice versa [39]. Thus, we perform TFBG calibration in the RI range for biological tissues and analyze the cladding mode resonances behavior during LA.

Moreover, we propose the reconstruction algorithm based on coupled-mode theory for measuring a quasi-distributed temperature profile along the TFBG during LA. The initial version of the algorithm has been already validated by our group for linearly chirped FBG (CFBG). CFBG is a fiber structure with the grating period linearly increased along the grating length, which results in a broad reflection spectrum that can be from a few to tens of nanometers in full-width half-maximum (FWHM) bandwidth [23]. The algorithm has been validated for measurements during LA using commercial CFBGs [40], [41], and using a custom-made plastic CFBG [42]. A detailed description of the CFBG spectrum model and related temperature profile reconstruction is provided in [43].

It is important to note that this algorithm is challenging to use for TFBG due to the small amplitude and narrow bandwidth of the TFBG's core mode. Thus, in this work, we modify the algorithm and validate it by comparing its results with the conventional core mode tracking techniques and the FBG array measurements.

II. Materials and Methods

A. Fiber Optic Interrogation System

The Micron Optics si255 optical interrogator (*Micron Optics*, Atlanta, USA) was utilized to measure the spectra of

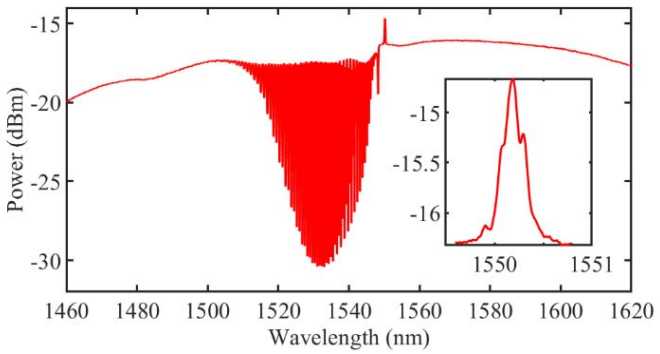

Fig. 1. The spectrum of a 10 mm – long TFBG with an 8° tilt angle; inset reports the core mode of TFBG (centered at 1550 nm).

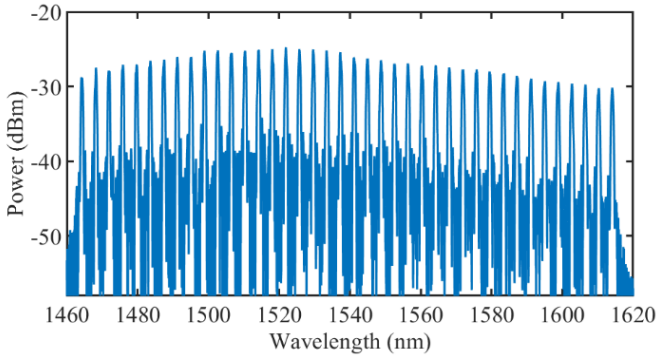

Fig. 2. Custom-made FBG array reflection spectrum: 40 FBG peaks at the range of 1460-1620 nm.

the FBG array and the TFBG with a 10 Hz sampling rate, with a synchronized approach. Both ends of TFBG were connected to two different channels of the interrogator and the overall "transmission-reflection" spectrum was measured.

B. Tilted Fiber Bragg Grating

For this work, we utilized commercially available TFBG (*Technica Optical Components*, Atlanta, USA) with an 8° tilt angle, a 10 mm grating length, apodized FBG profile, and core mode at 1550 nm with FWHM less than 0.5 nm. Fig. 1 reports the overall "transmission-reflection" spectrum of the TFBG sensor: the core mode centered at 1550 nm, the ghost mode at 1548 nm, and the cladding mode resonances comb is approximately in the range of 1509 nm – 1547 nm.

Moreover, separate calibrations specific for each sensing modality were performed: the core-to-core Bragg resonance calibration for temperature sensing, and RI calibration of the cladding mode resonances comb for RI sensing.

The core-to-core Bragg resonance of the TFBG was calibrated in the temperature range from 34 °C to 50 °C, where a T-type thermocouple was used as a reference temperature sensor. As a result, the core mode's temperature sensitivity of the TFBG is $(7.05 \pm 0.01)\times10^{-6}$ °C^{-1}.

C. Fiber Bragg Grating Array

For reference temperature measurements, the custom-made highly dense FBG array was fabricated with femtosecond point-by-point writing technique in polyimide-coated single-mode fiber SM1500(9/125)P with a reduced coating diameter of 145 μm (Fibercore Ltd., Southampton, UK). The array consists of 40 FBGs uniformly positioned along the sensing length of 48 mm (grating length is 1.15 mm, edge-to-edge distance is 0.05 mm), the reflection coefficients of FBGs are about 10-20 %, which allows a high dynamic range (>30 dB). Fig. 2 reports the reflected spectrum of the FBG array.

FBG properties were optimized to provide high spatial resolution and a high-quality spectrum for accurate temperature measurements of high-gradient temperature profiles possible during LA [18]. In addition, polyimide coating allows high-temperature measurements (> 400 °C for a short duration) [44]–[46]. The temperature sensitivity of the array

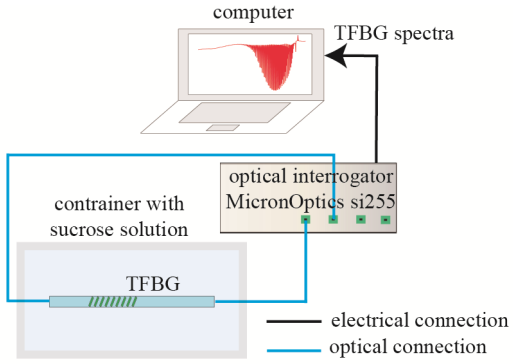

Fig. 3. Experimental setup for TFBG calibration using sucrose solutions with different concentrations in the range of 12 % - 60 % (1.333 RIU - 1.4419 RIU, referenced at 589 nm).

is $(7.43 \pm 0.01)\times10^{-6}$ °C$^{-1}10^{-6}$ °C^{-1}. Detailed information about the fabrication and metrological aspects of the FBG array is provided in the previous works of the group [29], [46].

D. RI Calibration of TFBG Sensor

In order to analyze the effect of different RI on TFBG spectra, calibration of TFBG in different sucrose concentrations was performed. The sucrose solutions were used with a concentration range from 0% to 60% with a step of 6% and corresponding to the RI range from 1.333 RIU to 1.4419 RIU (refractive index units), which is the typical range of RI for biological tissues [47], [48]. The different solutions were injected inside the container where the TFBG was placed. After each sucrose concentration, the TFBG and the container were rinsed with distilled water. Three calibration tests were performed. Fig. 3 illustrates the schematics of the experimental setup used for RI calibration.

E. Laser Ablation

Interstitial LA experiments were performed on *ex vivo* healthy porcine liver tissue, which was obtained from a local farm. The initial temperature of the liver, corresponding to 22.0 ± 0.5 °C, was measured with a thermocouple before each experiment.

The developed system consists of the laser diode and the Micron Optics interrogator, both connected to a computer where a custom-made LabVIEW program was used to start

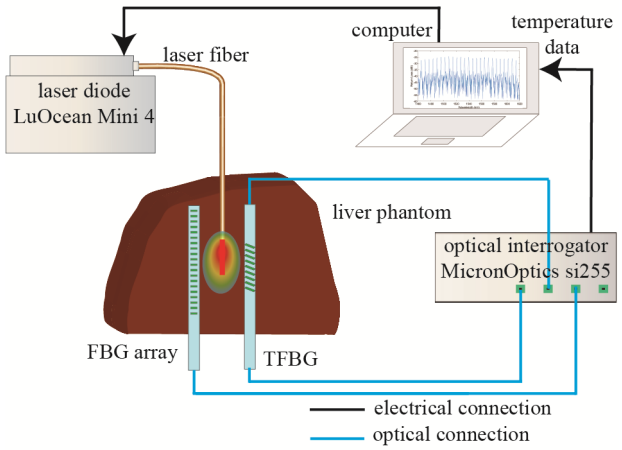

Fig. 4. Experimental setup for LA ablation: TFBG sensor and FBG array were placed at a 2 mm distance from the applicator on one half of *ex vivo* porcine liver. After, the second half of liver covers sensors and applicator in a "sandwich" approach.

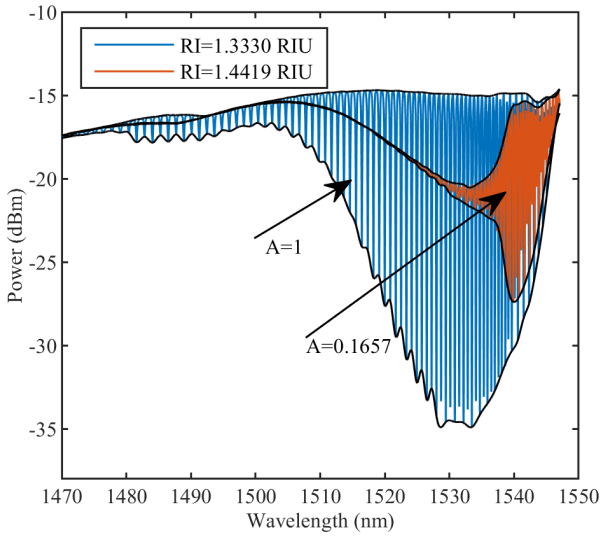

Fig. 5. The cladding mode resonances comb of TFBG positioned in water (blue line, RI = 1.333 RIU) and in a 60 % sucrose solution (red line, RI = 1.4419 RIU); related normalized area *A* decreases from 1.00 (reference value, RI = 1.333 RIU) to 0.1657 (RI=1.4419 RIU).

laser ablation and perform monitoring of the FBG array and TFBG spectra.

The diode laser (LuOcean Mini 4, Lumics, Berlin, Germany) working in continuous-wave mode at a 1064 nm wavelength and 2.6 W power was used for the thermal treatment. This wavelength belongs to the "therapeutic window" largely used for assuring the overall absorption of the laser light by the biological tissues, thus, entailing the temperature increase necessary for the thermal therapy. Moreover, the program automatically switched off the laser after the preset time or if the temperature measured by the FBG array exceeded 300 °C. This operation is done for preserving the sensing fibers from thermal damage.

The 400 μm laser guiding fiber with the commercial diffuser (Molex, Lisle, USA) at the tip was utilized to obtain uniform tissue damage around it. The diffuser has a low OH core, a diameter of 400 μm, and a length of 10 mm. It is worth noting that the diffuser leads to a decrease of spatial thermal gradients exposed to the TFBG with respect to a standard bare fiber applicator [30]. Thus, TFBG's core mode shape changes are smaller and the possibility of the error in temperature reconstruction is minimized.

Liver tissue was cut into two halves, then the applicator and the sensors were positioned on the surface of one half (Fig. 4); after they were covered with another half in a "sandwich" approach. This approach is largely used to accurately control the relative positions of the applicator and sensors within the biological tissues [24]. The TFBG sensor and the FBG array were placed parallel to the applicator at different sides; the distance from the sensors to the applicator was 2 mm. Indeed, being the liver tissue highly homogeneous, we assumed the spatial distribution of the laser-induced temperature to be symmetric on the application plane.

F. Data Analysis

1) Cladding Mode Resonances Analysis: It is important to note that the standard approach of peak tracking of the cladding mode resonances is not effective for a wide range of RI [49]. Indeed, each mode is resonant and more sensitive to the specific range of RI, and its sensitivity decreases significantly for a high RI range. For a high RI range, the cladding mode resonance has to be visible for all RI values, hence positioned at low-order modes, at a higher wavelength (at about 1535 nm in Fig. 5), so such mode resonance is positioned far from the cut-off point and the overall RI sensitivity is low.

Therefore, the envelope method, firstly proposed in [50], was utilized for the RI measurements. This method is based on the determination of the lower and upper envelope curves of the TFBG cladding mode resonances comb, and then evaluation of the normalized area A between the envelopes. As RI increases, more modes become lossy leading to cladding mode resonances decreasing and bringing together the lower and the upper envelopes. Thus, the normalized area decreases too. As a result, the normalized area evolution can be correlated to the RI changes [50]. Fig. 5 illustrates the main principle of this correlation: the cladding modes and the normalized area A are changed for RI increase from 1.3330 to 1.4416 RIU.

2) Core Mode: Conventional Peak Tracking: In our work, initially, the peak of the core mode is tracked with three conventional direct methods: maximum tracking, X-dB Bandwidth, and centroid [51].

For maximum tracking, the wavelength that corresponds to the maximum amplitude is detected as the core mode Bragg wavelength.

For X-dB Bandwidth, the inner bandwidth is defined as X dB below the maximum value; then, the center of the inner bandwidth is measured as the Bragg wavelength.

For the centroid method, the Bragg wavelength is estimated as the center of the mass of the FBG reflection spectrum according to the (1):

$$\lambda_{B,e} = \frac{\sum_n \lambda_n \times R(\lambda_n)}{\sum_n R(\lambda_n)} \tag{1}$$

where index n sweeps the main portion of the core mode spectrum.

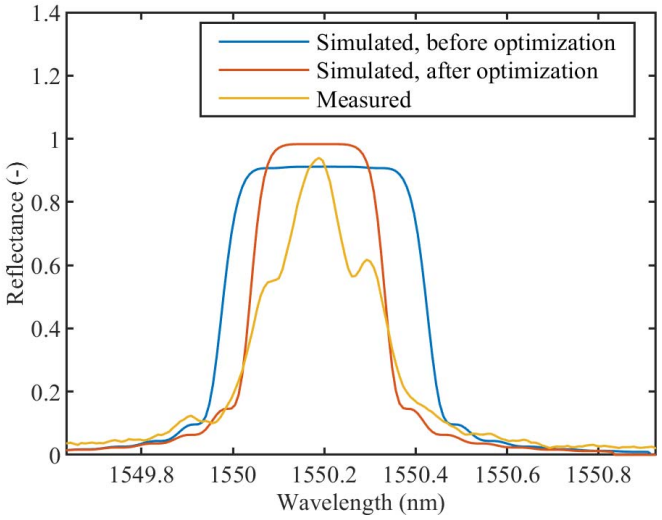

Fig. 6. TFBG core mode spectra: modeled before optimization (blue line), after optimization (red line), and normalized TFBG core mode measured with MicronOptics si255 (yellow line).

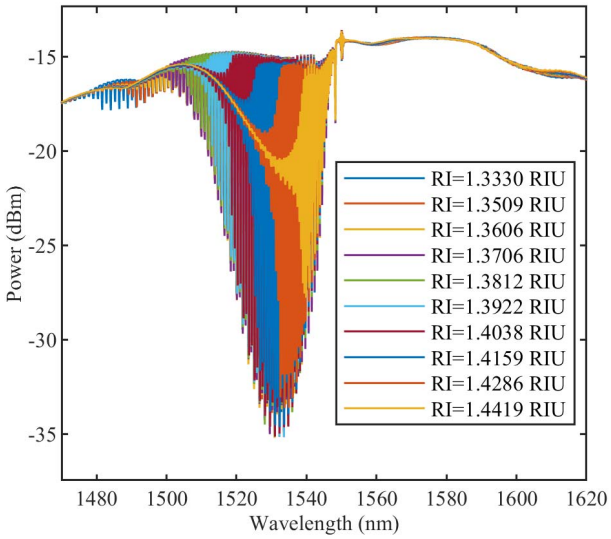

Fig. 7. TFBG spectra for different sucrose concentrations and related RI values (measured at room temperature).

3) Core Mode: Reconstruction Algorithm: The algorithm used for TFBG temperature profile reconstruction is based on the CFBG reconstruction algorithm devised in our previous works [43], [52]. The main idea remains the same: the spectrum (of the TFBG, for this work) is modeled as a chain of FBGs using coupled mode theory [23], then the iterative approach is utilized to minimize the mismatch between the real measured TFBG spectrum and the TFBG model perturbated by Gaussian-shaped temperature profiles. Afterward, the temperature profile, which corresponds to the smallest mismatch, is defined as temperature along the TFBG.

However, it is important to notice that the CFBG spectra described in [43], [52] have higher amplitude and bandwidth than TFBG. Indeed, Fig.1 zoom-in reports that the measured core mode of TFBG (yellow line) has approximately 1 nm bandwidth and several dBm from the peak to the base. As a result, temperature reconstruction for TFBG is more challenging than for CFBG.

In this regard, we propose to optimize the method reported in [43] by iterative optimization of the bandwidth of the core mode for spectrum modeling. In other words, the edges of the modeled spectrum are not defined manually according to the measured spectrum but automatically adjusted, to minimize the difference between the measured spectrum and the modeled one. Fig. 6 illustrates the obtained results for spectrum modeling and related measured spectrum. After this bandwidth optimization, the remaining steps follow the same approach as in the CFBG reconstruction algorithm discussed in detail in [43]. The results of TFBG profile reconstruction were compared with FBG array data and TFBG core mode tracking using root-mean-square error (RMSE).

III. Results

A. Calibration of TFBG Sensor for Different RI

The TFBG spectra for different sucrose concentrations from 0 % to 60 % (1.333 RIU to 1.4419 RIU) are reported in Fig. 7. As it can be clearly seen, the shape of the spectrum is significantly changed: the cut-off region starts approximately at 1530 nm for 60 % sucrose concentration and the high-order modes become lossy. The obtained RI calibration results using the envelope method (the normalized area was measured in the spectral region between 1470 nm and 1547 nm) are in accordance with the results in [50] (Fig. 8), in which TFBGs with different tilt angles were calibrated for surrounding RI sensing.

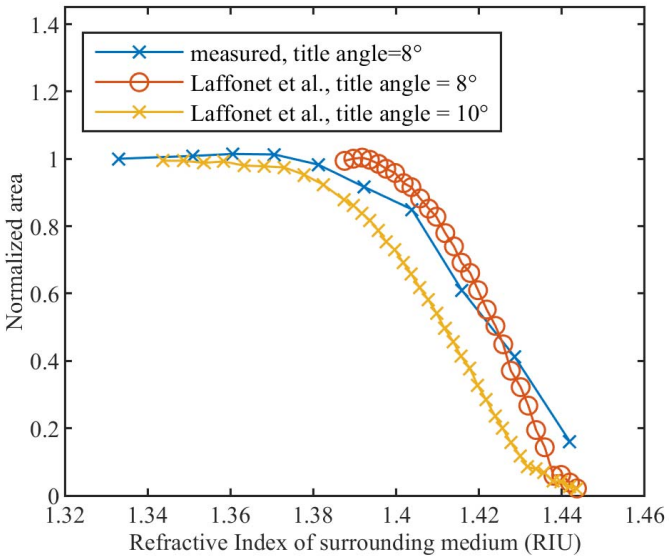

Fig. 8. Calibration of RI sensing with envelope method: average results of three calibration experiments (blue line with X marker). The obtained data is in accordance with Laffonet *et al. al.* [50], in which RI calibration of different TFBGs was performed.

B. Analysis of the Cladding Mode Resonances During LA

Fig. 9 top illustrates TFBG spectra changes during LA of *ex vivo* liver at different time instants: before the start of ablation (t=0 s), after 90 s, and at the moment when the laser was switched off (t=180 s). Both the amplitude of the cladding mode resonances and the upper and lower

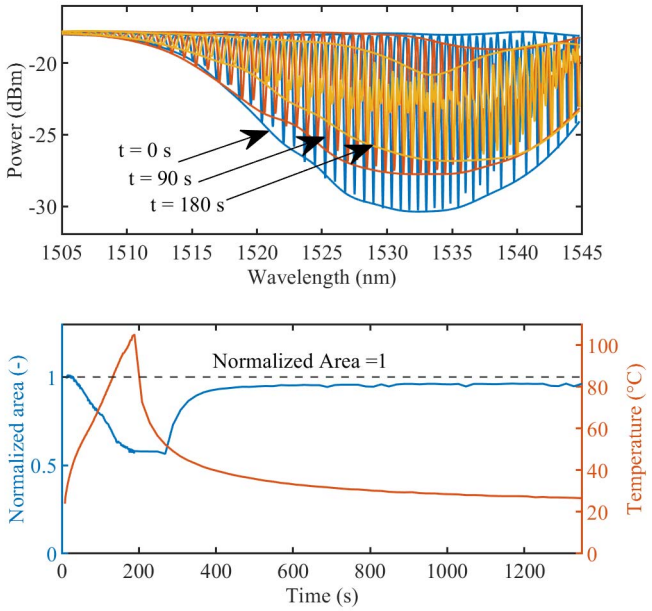

Fig. 9. (top) TFBG spectra measured during LA of *ex vivo* porcine liver at different time instances: before the laser ablation at t=0 s (blue color); at t – 90 s (red color), and when laser was switched off t=180 s. Amplitude changes of spectra, and related shape changes, can be seen. (bottom) Normalized area evolution (left y-axis) and temperature change measured by FBG array (right y-axis) during LA experiment.

envelopes of the spectra change during LA. The normalized area between two envelopes (left y-axis) and related temperature changes measured by the FBG array (right y-axis) are presented in Fig. 9 bottom. As can be seen, the trend of temperature evolution can be approximately correlated with the changes in the normalized area (Fig. 9 bottom). Thus, ideally, we expect to obtain information about the maximum temperature from the minimum value of the normalized area. Moreover, after complete cooling, the normalized area is expected to be correlated with the RI change of the ablated tissue.

However, the results show that the repeatability of the experimental trials is low. As a result, it is very challenging to obtain useful information about temperature and RI changes from the cladding comb analysis. For instance, Fig. 10 reports the relation between maximum temperature measured by TFBG (using maximum peak tracking) and the related minimum value of the normalized area for each of 25 experimental trials. As expected, higher temperature leads to a smaller area between envelopes. Indeed, Fig. 10 shows that for the experiments with low maximum temperatures ($\sim$ 26 °C) the related normalized area is very close to 1 because there is no significant shift and amplitudes decrease of the cladding mode resonances. However, due to the high value or RMSE between the fitting and the measured data (RMSE = 0.148), the temperature cannot be accurately correlated with the normalized area (Fig. 10).

Moreover, due to the high effect of temperature on the cladding comb, RI changes of the tissues after LA are challenging to measure too. The possible reasons for the low efficacy of cladding comb analysis during LA are provided in the discussion section.

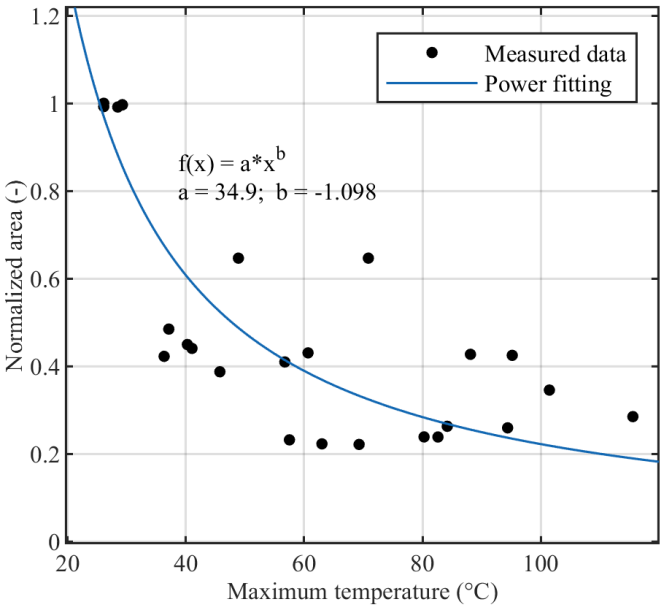

Fig. 10. Relation between maximum temperature measured by TFBG (using maximum peak tracking) and related minimum value of normalized area for each of 25 experimental trials. RMSE between data and fitting is 0.148.

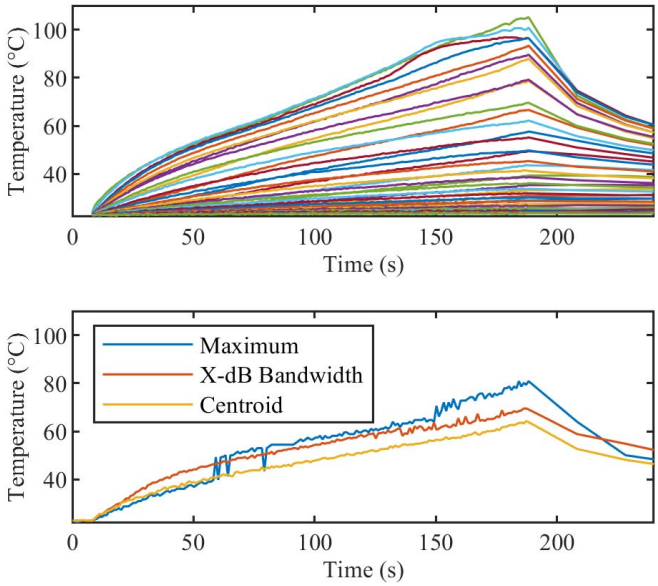

Fig. 11. (top) FBG array temperature for 40 gratings during laser ablation; (bottom) temperature reconstructed using analysis of core mode with direct peak-tracking techniques: maximum, X-dB Bandwidth (where X is −5 dB), centroid.

C. Analysis of the Core Mode During LA

Fig. 11 top reports temperature evolution measured by the FBG array during one experiment. The maximum temperature reached after 180 s of ablation is 105.2 °C. At the same moment, the TFBG core mode shows 80.9 °C measured by maximum peak tracking, 69.5 °C by X-dB Bandwidth, and 64.3 °C by the centroid method. The RMSE between maximum temperatures measured by FBG array and TFBG (maximum peak tracking) is 18.31 °C.

Fig. 12 and 13 report the results of the temperature profile along the TFBG using the proposed algorithm. Fig.12 shows

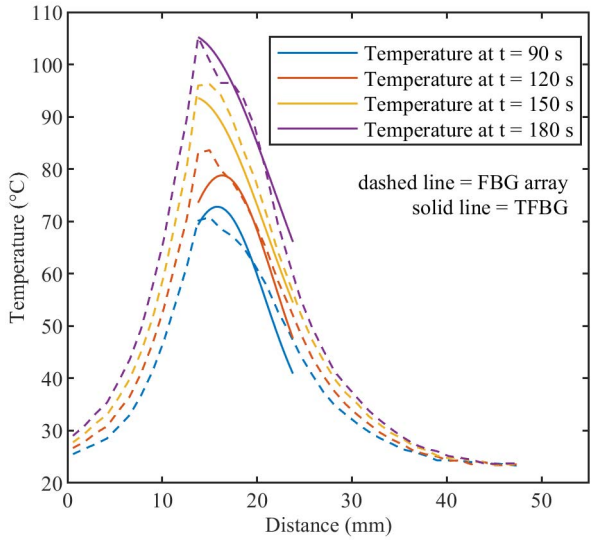

Fig. 12. Measurements during LA experiment at different time instants: dashed lines – FBG array temperature measurements, solid lines – reconstructed TFBG temperature profiles (normalized).

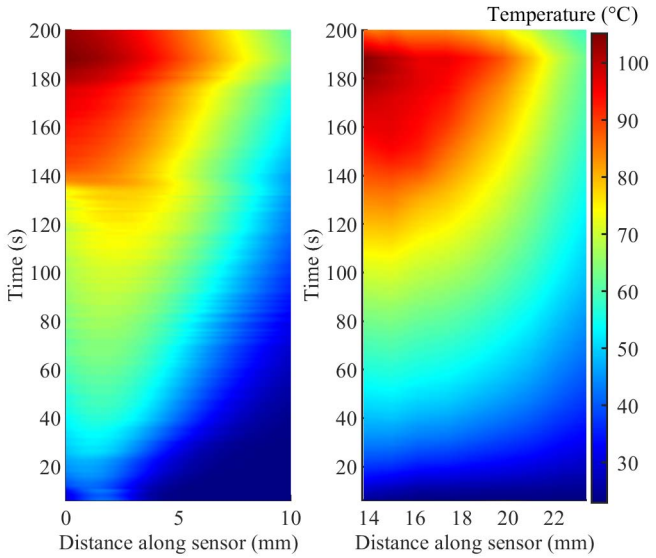

Fig. 13. Measurements during LA experiments: (a) FBG array; (b) TFBG temperature obtained by the proposed algorithm. The RMSE between FBG array and TFBG profile measurements for three experiments is 7.8±1.7 °C.

the temperature measured by the FBG array (dashed line) and temperature reconstructed along the TFBG (solid line) at different time moments. For this figure, to clearly illustrate the algorithm's ability to reconstruct profile trends, TFBG temperature was normalized to the maximum temperature measured by the FBG array. Fig. 13 reports temperature evolution for both sensors during laser ablation of the tissue. The RMSE between the FBG array and TFBG measurements for three experiments is 7.8±1.7 °C.

IV. Discussion

In general, the initial hypothesis was to obtain information about the RI of the ablated tissue using the cladding mode resonance tracking, while the temperature effect on the cladding mode resonances is compensated by temperature measured by the core mode tracking. However, the experiments showed that the cladding comb changed significantly during LA (high wavelength shift and appearance of leaky modes). Thus, the cladding resonances tracking was not possible. Indeed, it is in agreement with [50]: distinct temperature sensitivity of cladding modes leads not only to the shift of the cladding mode resonances, but to the change of the shape of the TFBG spectrum under temperature elevation. Thus, the envelope method was utilized to measure the area between upper and lower envelopes of the TFBG cladding resonances comb during LA.

However, the results show that temperature and RI information is not possible to accurately measure by the cladding comb analysis. The possible reasons can be inhomogeneity and structure of the tissue that does not allow ideal contact between the sensor surface and the tissue, the change of the TFBG surface after each experiment (even considering that TFBG was cleaned after each trial). Moreover, bending, strain, and humidity also have a cross-sensitivity effect on the shape of the TFBG spectrum [32], which makes RI measurements using the envelope method even more challenging.

As a result, we conclude that the main sensing modality of TFBG is temperature measurements based on the core mode analysis. The resulted RMSE of 7.8±1.7 °C between TFBG profile reconstruction and FBG reference measurements can be mostly explained by the positioning of the sensors on the opposite sides of the diffuser and the high thermal gradients associated with LA. For future characterization of TFBG temperature measurements, the reference sensor and FBG should have the same exact placing, preferably in capillary or tubing to eliminate cross-sensitivity effects from other intra-tissue parameters.

The TFBG temperature sensor analyzed by conventional methods has several disadvantages over Rayleigh-based distributed sensing and FBG measurements: one-point measurement, averaging over the TFBG length (∼ 1 cm), fragility (TFBG usually does not have a coating to allow coupling with leaky modes). However, a TFBG can be used as a sensor and a heat source, as proposed in a recent study [4]. In this regard, sensing modalities and capabilities of TFBG during LA need to be analyzed in detail, and this work can be considered a step toward such analysis.

V. Conclusion

In this work, we have implemented a temperature profile reconstruction algorithm for TFBG and validated it during LA in *ex vivo* liver. The algorithm is based on modeling the TFBG core mode as a chain of FBGs, each sensitive to a local temperature shift. Afterward, the iterative optimization method is used to define the temperature profile along the TFBG. The obtained results were compared with direct peak-tracking techniques (maximum tracking, X-dB Bandwidth, centroid methods) used to measure the core mode shift of TFBG, and with FBG array measurements. In addition, the cladding mode resonances behavior for different sucrose concentrations, and then during LA was investigated. In general, the proposed reconstruction algorithm provides 7.8±1.7 °C RMS error with respect to the FBG array temperature measurements and can

be effective for real-time TFBG temperature profile measurements during LA ablation.

ACKNOWLEDGMENT

The authors would like to thank Annalisa Orrico, Giulia Saudelli, and Leonardo Pascucci for the help provided during the experiments.

Sanzhar Korganbayev, Martina De Landro, and Paola Saccomandi are with the Department of Mechanical Engineering, Politecnico di Milano, 20156 Milan, Italy (e-mail: sanzhar.korganbayev@polimi.it; martina.delandro@polimi.it; paola.saccomandi@polimi.it).

Alexey Wolf is with the Institute of Automation and Electrometry, Siberian Branch of the Russian Academy of Sciences, 630090 Novosibirsk, Russia (e-mail: wolf@iae.nsk.su).

Daniele Tosi is with the Biosensors and Bioinstrumentation Laboratory—National Laboratory Astana, 010000 Nur-Sultan, Kazakhstan, and also with the School of Engineering and Digital Sciences, Nazarbayev University, 010000 Nur-Sultan, Kazakhstan (e-mail: daniele.tosi@nu.edu.kz).

REFERENCES

[1] C. J. Diederich, "Thermal ablation and high-temperature thermal therapy: Overview of technology and clinical implementation," *Int. J. Hyperthermia*, vol. 21, no. 8, pp. 745–753, 2005.

[2] S. Sartori, F. Di Vece, F. Ermili, and P. Tombesi, "Laser ablation of liver tumors: An ancillary technique, or an alternative to radiofrequency and microwave?" *World J. Radiol.*, vol. 9, no. 3, p. 91, 2017, doi: 10.4329/wjr.v9.i3.91.

[3] D. Kalamida, I. V. Karagounis, A. Mitrakas, S. Kalamida, A. Giatromanolaki, and M. I. Koukourakis, "Fever-range hyperthermia vs. hypothermia effect on cancer cell viability, proliferation and HSP90 expression," *PLoS ONE*, vol. 10, no. 1, Jan. 2015, Art. no. e0116021.

[4] S. A. Alqarni, W. G. Willmore, J. Albert, and C. W. Smelser, "Self-monitored and optically powered fiber-optic device for localized hyperthermia and controlled cell death *in vitro*," *Appl. Opt.*, vol. 60, no. 8, pp. 2400–2411, 2021.

[5] M. G. Lubner, C. L. Brace, J. L. Hinshaw, and F. T. Lee, "Microwave tumor ablation: Mechanism of action, clinical results, and devices," *J. Vascular Interventional Radiol.*, vol. 21, no. 8, pp. S192–S203, Aug. 2010, doi: 10.1016/j.jvir.2010.04.007.

[6] S. N. Goldberg, "Radiofrequency tumor ablation: Principles and techniques," in *Multi-Treatment Modalities of Liver Tumours*. Boston, MA, USA: Springer, 2002, pp. 87–118.

[7] Y.-F. Zhou, "High intensity focused ultrasound in clinical tumor ablation," *World J. Clin. Oncol.*, vol. 2, no. 1, p. 8, 2011, doi: 10.5306/wjco.v2.i1.8.

[8] R. J. Stafford, D. Fuentes, A. A. Elliott, J. S. Weinberg, and K. Ahrar, "Laser-induced thermal therapy for tumor ablation," *Crit. Rev. Biomed. Eng.*, vol. 38, no. 1, pp. 79–100, 2010, doi: 10.1615/CritRevBiomedEng.v38.i1.70.

[9] F. Manns, P. J. Milne, X. Gonzalez-Cirre, D. B. Denham, J. M. Parel, and D. S. Robinson, "*In situ* temperature measurements with thermocouple probes during laser interstitial thermotherapy (LITT): Quantification and correction of a measurement artifact," *Lasers Surg. Med.*, vol. 23, no. 2, pp. 94–103, 1998, doi: 10.1002/(SICI)1096-9101(1998)23:2<94::AID-LSM7>3.0.CO.2-Q.

[10] C. M. Pacella *et al.*, "Thyroid tissue: U.S.-Guided percutaneous interstitial laser ablation—A feasibility study," *Radiology*, vol. 217, no. 3, pp. 673–677, Dec. 2000, doi: 10.1148/radiology.217.3.r00dc09673.

[11] H.-J. Schwarzmaier *et al.*, "MR-guided laser-induced interstitial thermotherapy of recurrent glioblastoma multiforme: Preliminary results in 16 patients," *Eur. J. Radiol.*, vol. 59, no. 2, pp. 208–215, Aug. 2006, doi: 10.1016/j.ejrad.2006.05.010.

[12] F. M. Di Matteo *et al.*, "Feasibility of EUS-guided Nd:YAG laser ablation of unresectable pancreatic adenocarcinoma," *Gastrointest. Endosc.*, vol. 88, no. 1, pp. 168–174.e1, Jul. 2018, doi: 10.1016/j.gie.2018.02.007.

[13] A. Gangi, H. Alizadeh, L. Wong, X. Buy, J.-L. Dietemann, and C. Roy, "Osteoid osteoma: Percutaneous laser ablation and follow-up in 114 patients," *Radiology*, vol. 242, no. 1, pp. 293–301, Jan. 2007, doi: 10.1148/radiol.2421041404.

[14] T. J. Vogl, R. Straub, K. Eichler, O. Söllner, and M. G. Mack, "Colorectal carcinoma metastases in liver: Laser-induced interstitial thermotherapy—Local tumor control rate and survival data," *Radiology*, vol. 230, no. 2, pp. 450–458, Feb. 2004, doi: 10.1148/radiol.2302020646.

[15] K. F. Chu and D. E. Dupuy, "Thermal ablation of tumours: Biological mechanisms and advances in therapy," *Nat. Rev. Cancer*, vol. 14, no. 3, pp. 199–208, 2014, doi: 10.1038/nrc3672.

[16] J.-T. Lin, Y.-S. Chiang, G.-H. Lin, H. Lee, and H.-W. Liu, "*In vitro* photothermal destruction of cancer cells using gold nanorods and pulsed-train near-infrared laser," *J. Nanomater.*, vol. 2012, pp. 1–6, Jul. 2012, doi: 10.1155/2012/861385.

[17] K. Ivarsson, J. Olsrud, C. Sturesson, P. H. Möller, B. R. Persson, and K. G. Tranberg, "Feedback interstitial diode laser (805 nm) thermotherapy system: *Ex vivo* evaluation and mathematical modeling with one and four-fibers," *Lasers Surg. Med.*, vol. 22, no. 2, pp. 86–96, 1998, doi: 10.1002/(SICI)1096-9101(1998)22:2<86::AID-LSM4>3.0.CO;2-S.

[18] A. J. Welch and M. J. C. C. Van Gemert, *Optical-Thermal Response of Laser-Irradiated Tissue*, vol. 2. Dordrecht, The Netherlands: Springer, 2011.

[19] P. Saccomandi, E. Schena, and S. Silvestri, "Techniques for temperature monitoring during laser-induced thermotherapy: An overview," *Int. J. Hyperthermia*, vol. 29, no. 7, pp. 609–619, Nov. 2013, doi: 10.3109/02656736.2013.832411.

[20] F. Morra *et al.*, "Spatially resolved thermometry during laser ablation in tissues: Distributed and quasi-distributed fiber optic-based sensing," *Opt. Fiber Technol.*, vol. 58, Sep. 2020, Art. no. 102295, doi: 10.1016/j.yofte.2020.102295.

[21] E. G. Macchi *et al.*, "Optical fiber sensors-based temperature distribution measurement in *ex vivo* radiofrequency ablation with submillimeter resolution," *Proc. SPIE*, vol. 19, no. 11, Nov. 2014, Art. no. 117004, doi: 10.1117/1.jbo.19.11.117004.

[22] Z. Ashikbayeva *et al.*, "Distributed 2D temperature sensing during nanoparticles assisted laser ablation by means of high-scattering fiber sensors," *Sci. Rep.*, vol. 10, no. 1, p. 12593, Dec. 2020, doi: 10.1038/s41598-020-69384-2.

[23] T. Erdogan, "Fiber grating spectra," *J. Lightw. Technol.*, vol. 15, no. 8, pp. 1277–1294, Aug. 1997, doi: 10.1109/50.618322.

[24] R. Gassino, Y. Liu, M. Konstantaki, A. Vallan, S. Pissadakis, and G. Perrone, "A fiber optic probe for tumor laser ablation with integrated temperature measurement capability," *J. Lightw. Technol.*, vol. 35, no. 16, pp. 3447–3454, Aug. 15, 2017, doi: 10.1109/JLT.2016.2618618.

[25] L. Bianchi *et al.*, "Fiber Bragg grating sensors-based thermometry of gold nanorod-enhanced photothermal therapy in tumor model," *IEEE Sensors J.*, vol. 22, no. 12, pp. 11297–11306, Jun. 2022, doi: 10.1109/JSEN.2021.3082042.

[26] N. D. Schulmann, M. Soltani-Sarvestani, M. De Landro, S. Korganbayev, S. Cotin, and P. Saccomandi, "Model-based thermometry for laser ablation procedure using Kalman filters and sparse temperature measurements," *IEEE Trans. Biomed. Eng.*, early access, Mar. 1, 2022, doi: 10.1109/TBME.2022.3155574.

[27] Y. Liu, R. Gassino, A. Braglia, A. Vallan, and G. Perrone, "Fibre probe for tumour laser thermotherapy with integrated temperature measuring capabilities," *Electron. Lett.*, vol. 52, no. 10, pp. 798–800, May 2016.

[28] S. Korganbayev, R. Pini, A. Orrico, A. Wolf, A. Dostovalov, and P. Saccomandi, "Towards temperature-controlled laser ablation based on fiber Bragg grating array temperature measurements," in *Proc. IEEE Int. Workshop Metrol. Ind. 4.0 IoT*, Jun. 2020, pp. 268–272, doi: 10.1109/MetroInd4.0IoT48571.2020.9138171.

[29] S. Korganbayev *et al.*, "Closed-loop temperature control based on fiber Bragg grating sensors for laser ablation of hepatic tissue," *Sensors*, vol. 20, no. 22, pp. 1–16, Nov. 2020, doi: 10.3390/s20226496.

[30] L. Bianchi, S. Korganbayev, A. Orrico, M. De Landro, and P. Saccomandi, "Quasi-distributed fiber optic sensor-based control system for interstitial laser ablation of tissue: Theoretical and experimental investigations," *Biomed. Opt. Exp.*, vol. 12, no. 5, p. 2841, May 2021, doi: 10.1364/BOE.419541.

[31] S. Korganbayev *et al.*, "PID controlling approach based on FBG array measurements for laser ablation of pancreatic tissues," *IEEE Trans. Instrum. Meas.*, vol. 70, pp. 1–9, 2021, doi: 10.1109/TIM.2021.3112790.

[32] J. Albert, L.-Y. Shao, and C. Caucheteur, "Tilted fiber Bragg grating sensors," *Laser Photon. Rev.*, vol. 7, no. 1, pp. 83–108, Jan. 2013.

[33] T. Guo, F. Liu, B.-O. Guan, and J. Albert, "Tilted fiber grating mechanical and biochemical sensors," *Opt. Laser Technol.*, vol. 78, pp. 19–33, Apr. 2016, doi: 10.1016/j.optlastec.2015.10.007.

[34] C. Leitao *et al.*, "Cortisol in-fiber ultrasensitive plasmonic immunosensing," *IEEE Sensors J.*, vol. 21, no. 3, pp. 3028–3034, Feb. 2020, doi: 10.1109/JSEN.2020.3025456.
[35] T. Zhu, M. Loyez, K. Chah, and C. Caucheteur, "Partially gold-coated tilted FBGs for enhanced surface biosensing," *Opt. Exp.*, vol. 30, no. 10, p. 16518, May 2022, doi: 10.1364/OE.458548.
[36] T. Osuch, T. Jurek, K. Markowski, and K. Jedrzejewski, "Simultaneous measurement of liquid level and temperature using tilted fiber Bragg grating," *IEEE Sensors J.*, vol. 16, no. 5, pp. 1205–1209, Mar. 2015.
[37] R. Agah, A. H. Gandjbakhche, M. Motamedi, R. Nossal, and R. F. Bonner, "Dynamics of temperature dependent optical properties of tissue: Dependence on thermally induced alteration," *IEEE Trans. Biomed. Eng.*, vol. 43, no. 8, pp. 839–846, Aug. 1996.
[38] M. De Landro *et al.*, "Prediction of *in vivo* laser-induced thermal damage with hyperspectral imaging using deep learning," *Sensors*, vol. 21, no. 20, p. 6934, Oct. 2021.
[39] M. E. Shvachkina, D. D. Yakovlev, A. B. Pravdin, and D. A. Yakovlev, "Average refractive index of tendon as a function of water content," *J. Biomed. Photon. Eng.*, vol. 4, no. 1, pp. 13–21, 2018.
[40] S. Korganbayev *et al.*, "Linearly chirped fiber-optic Bragg grating as distributed temperature sensor for laser ablation," in *Proc. IEEE SENSORS*, Oct. 2016, pp. 1–3, doi: 10.1109/ICSENS.2016.7808610.
[41] P. Saccomandi *et al.*, "Linearly chirped fiber Bragg grating response to thermal gradient: From bench tests to the real-time assessment during *in vivo* laser ablations of biological tissue," *J. Biomed. Opt.*, vol. 22, no. 9, p. 1, Sep. 2017, doi: 10.1117/1.jbo.22.9.097002.
[42] S. Korganbayev *et al.*, "Thermal profile detection through high-sensitivity fiber optic chirped Bragg grating on microstructured PMMA fiber," *J. Lightw. Technol.*, vol. 36, no. 20, pp. 4723–4729, Oct. 15, 2018, doi: 10.1109/JLT.2018.2864113.
[43] S. Korganbayev *et al.*, "Detection of thermal gradients through fiber-optic chirped fiber Bragg grating (CFBG): Medical thermal ablation scenario," *Opt. Fiber Technol.*, vol. 41, pp. 48–55, Mar. 2017, doi: 10.1016/j.yofte.2017.12.017.
[44] T. G. Giallorenzi and A. Dandridge, *Optical Fiber Sensor Technology*, vol. 3. Boston, MA, USA: Springer, 1987.
[45] L. Huang, R. S. Dyer, R. J. Lago, A. A. Stolov, and J. Li, "Mechanical properties of polyimide coated optical fibers at elevated temperatures," *Proc. SPIE*, vol. 9702, Mar. 2016, Art. no. 97020Y, doi: 10.1117/12.2210957.
[46] A. V. Dostovalov, A. A. Wolf, A. V. Parygin, V. E. Zyubin, and S. A. Babin, "Femtosecond point-by-point inscription of Bragg gratings by drawing a coated fiber through ferrule," *Opt. Exp.*, vol. 24, no. 15, p. 16232, Jul. 2016, doi: 10.1364/OE.24.016232.
[47] R. Khan, B. Gul, S. Khan, H. Nisar, and I. Ahmad, "Refractive index of biological tissues: Review, measurement techniques, and applications," *Photodiagnosis Photodynamic Therapy*, vol. 33, Mar. 2021, Art. no. 102192.
[48] *Refractometer*. Accessed: Mar. 8, 2022. [Online]. Available: http://www.refractometer.pl/refraction-datasheet-sucrose
[49] S. Korganbayev *et al.*, "Optimization of cladding diameter for refractive index sensing in tilted fiber Bragg gratings," *Sensors*, vol. 22, no. 6, p. 2259, Mar. 2022, doi: 10.3390/s22062259.
[50] G. Laffont and P. Ferdinand, "Tilted short-period fibre-Bragg-grating-induced coupling to cladding modes for accurate refractometry," *Meas. Sci. Technol.*, vol. 12, no. 7, pp. 765–770, Jul. 2001, doi: 10.1088/0957-0233/12/7/302.
[51] D. Tosi, "Review and analysis of peak tracking techniques for fiber Bragg grating sensors," *Sensors*, vol. 17, no. 10, p. 2368, 2017.
[52] R. Min *et al.*, "Largely tunable dispersion chirped polymer FBG," *Opt. Lett.*, vol. 43, no. 20, p. 5106, Oct. 2018, doi: 10.1364/OL.43.005106.

Sanzhar Korganbayev (Member, IEEE) received the B.S. and M.S. degrees in electrical and electronics engineering from Nazarbayev University, Nur-Sultan, Kazakhstan, in 2016 and 2018, respectively. He is currently pursuing the Ph.D. degree with the Department of Mechanical Engineering, Politecnico di Milano. He is also involved in the LASER OPTIMAL Project (European Research Council Grant) for the development of software for real-time temperature monitoring and intraoperative adjustment of the laser ablation settings during tumor treatment. His research interests include fiber optic sensors and their applications for thermal and mechanical measurements.

Martina De Landro (Member, IEEE) received the M.S. degree in biomedical engineering from the Università Campus Bio-Medico di Roma. She is pursuing the Ph.D. degree in mechanical engineering. She performed her M.S. thesis at the IHU of Strasbourg, where she investigated the use of fiber optic sensors for catheters tracking. Her work focuses on the investigation of sensors and innovative images-based techniques for the monitoring of thermal outcome in tissues undergoing laser ablation.

Alexey Wolf received the M.Sc. degree in physics from Novosibirsk State University (NSU) in 2013 and the Ph.D. degree in optics from the Institute of Automation and Electrometry of the SB RAS (IAE SB RAS) in 2020. He currently works as a Researcher with the Laboratory of Nonlinear Waveguide Systems, NSU and the Laboratory of Fiber Optics, IAE SB RAS, where he develops new types of fiber lasers and sensors based on specialty optical fibers. His scientific interests include femtosecond laser micromachining, fiber Bragg gratings, and new optical materials.

Daniele Tosi received the B.Sc. and M.Sc. degrees in telecommunication engineering and the Ph.D. degree in electrical and computer engineering from the Politecnico di Torino in 2004, 2006, and 2010, respectively. He is an Associate Professor of Electrical and Computer Engineering with Nazarbayev University and the Head of the Biosensors and Bioinstruments Laboratory and the National Laboratory Astana. He is an Associate Editor of the IEEE SENSORS JOURNAL. He was a recipient of the IEEE Sensors Council Early Career Technical Award in 2018. His research interests include optical fiber sensors, biomedical sensors, distributed sensing, and biosensors.

Paola Saccomandi (Senior Member, IEEE) received the Ph.D. degree in biomedical engineering from the Università Campus Bio-Medico di Roma in 2014. From 2016 to 2018, she was a Postdoctoral Researcher with the IHU—Institute of Image-Guided Surgery of Strasbourg. Since 2018, she has been an Associate Professor with the Department of Mechanical Engineering, Politecnico di Milano. She is the Principal Investigator of the European Research Council Grant LASER OPTIMAL. The main research interests of Prof. Saccomandi and her team include fiber optic sensors, biomedical imaging, and the development of light-based approaches for hyperthermal tumor treatment and monitoring.